Hydration of hydrophobic biological porphyrins

T. R. Cuya Guizado,[1,a)] S. R. W. Louro,[1] and C. Anteneodo[1,2]
[1]*Departamento de Física, PUC-Rio, Rio de Janeiro, Brazil*
[2]*National Institute of Science and Technology for Complex Systems, Rio de Janeiro, Brazil*

(Received 1 October 2010; accepted 31 December 2010; published online 1 February 2011)

Explicit solvent, single solute molecular dynamics simulations of protoporphyrin IX and its Fe^{2+} complex (heme) in water were performed. The relation of solute–solvent was examined through the spatial distribution functions of water molecules around the centroid of the porphyrin ring. A detailed description of the time-averaged structure of water surrounding the solutes as well as of its fluctuations is presented. © *2011 American Institute of Physics*. [doi:10.1063/1.3544376]

I. INTRODUCTION

Protoporphyrin IX (PPIX) is produced within mitochondria and is the precursor of the heme synthesis. It has a central role in the photodynamic therapy against cancer, since PPIX generated from δ-aminolevulinic acid has been extensively used as an endogenous photosensitizer, leading to singlet oxygen production followed by cellular death of the surrounding tumoral tissue. The heme results from the complexation of PPIX with Fe^{2+}. Heme is the prosthetic group of a class of metalloproteins named hemoproteins. Myoglobin and hemoglobin accommodate heme in hydrophobic cavities. Due to the capacity of the heme iron atom to bind oxygen, such proteins can store and transport oxygen throughout the body. Cytochromes are also hemoproteins and are involved in the transfer of electrons in mitochondria, which is a fundamental process for supplying energy to the cell, and hence, for life. The structures of PPIX and heme are depicted in Fig. 1.

A crucial issue to understand the performance of porphyrins in biological systems, as well as for any other biomolecule, is to know the structural and dynamical properties of the surrounding water. As a matter of fact, the hydropathicity profile of a biomolecule strongly influences its hydrodynamics, aggregation properties, association of ligands, interaction with biomembranes, binding to receptors in proteins, etc. More specifically, the complex heme-water has been observed in several proteins. In bovine lactoperoxidase, water plays an important role, given that the protein activity is lowered when water is displaced by certain ligands.[1] In the case of Cytochrome P450s, iron spin state is mainly ruled by the iron-water distance.[2] X-ray diffraction also showed that there exists at least one water molecule present at the hydrophobic binding site of the heme in human serum albumin.[3]

Both PPIX and heme are known to be hydrophobic molecules. Preliminary molecular dynamics studies, where radial distribution functions (RDFs) were computed around various groups of both solutes, have confirmed the expectation that the hydrophobic character of porphyrins resides on the central ring, whereas the tails have a well defined hydrophilic profile.[4,5] However, RDFs provide only averaged information and miss important details of the water structure around a solute. In the present work, from the outcomes of molecular dynamics (MD) simulations in a classical approximation, spatial distribution functions were analyzed to obtain detailed information on the water structure surrounding PPIX and heme.

II. METHODS

A. Molecular dynamics

Molecular dynamics simulations were performed using the GROMACS3.2 (Ref. 6) package. Each single solute was inserted in a cubic box (at a distance of 1.2 nm from box walls) with more than 2000 explicit water molecules, using periodic boundary conditions. Because the studied porphyrins have charge −2 (in electron charge units) in physiological pH, the solutions were balanced with two Na^+ counterions.

The porphyrins were modeled in the GROMOS96 (53a6) force field, while charges were obtained by *ab initio* calculations in preliminary work.[4] The simple point charge model (SPC)[7] was used for water. To analyze model dependence, we also performed simulations for the heme using an all-atom force field (CHARMM27) and different models for water: SPC and SPCE (simple point charge extended model)[8] for GROMOS96 and SPC, SPCE, TIP3P, and TIP4P[9] for CHARMM27.

For the treatment of long-range electrostatic interactions, the particle mesh Ewald method was employed.[10] For both van der Waals and Coulomb interactions, a cut-off of 1.0 nm was used.

The systems were run in a NPT ensemble (fixed number of atoms, pressure and temperature), coupling the system with a Berendsen-thermostat to a 310 K thermal bath and the pressure was controlled with the Berendsen-barostat using a reference pressure of 1 atm.[11] In order to equilibrate the system, standard steps of energy minimization and equilibration of the system were followed prior to recording the useful MD simulations.[4] Finally, 10 ns MD simulations were performed to obtain the useful data. The trajectories were computed at every 2 fs and recorded every 1 ps.

a)Author to whom correspondence should be addressed. Electronic mail: teobaldo.ricardo@fis.puc-rio.br.

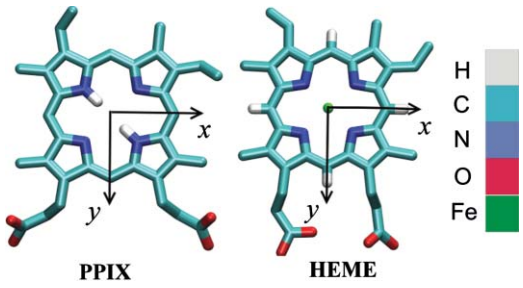

FIG. 1. The two porphyrins under study.

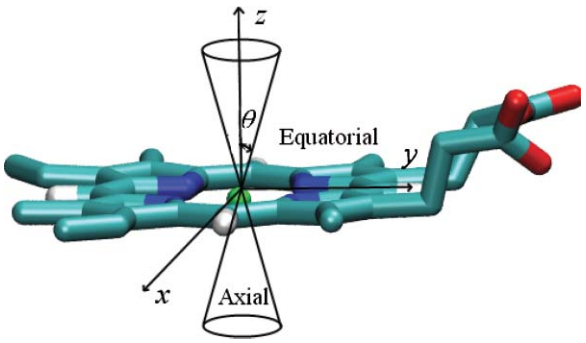

FIG. 2. Reference axes used in the computation of the distribution functions of water molecules. The origin of coordinates is at the CM of the four nitrogen atoms and the xy plane resides on the average ring plane.

B. Radial, axial, and equatorial distribution functions

The RDF $g(r)$ is one of the tools traditionally used to analyze the solute–solvent relation. It gives information about the distribution of particles as a function of the distance from a given point. The evaluation of the RDF displays the allocation of water molecules in the coordination shells around either the center of mass (CM) or chosen atoms of the solute, allowing us to detect the hydropathic pattern associated to each portion of the porphyrin as well as to the solute as a whole. However, $g(r)$ misses the angular distribution of the solvent. Thus, in order to gain further information on the distribution of water, but without excessive fine graining, which introduces noise, we divided the space in axial and equatorial regions, following the work by Rashke and Levitt,[12] based on the almost planar structure of the central ring. According to the Cartesian coordinate system in Fig. 2, the axial region is delimited by the cones defined by the points with polar angle θ from the positive and negative z-semiaxes, while the outer volume defines the equatorial region. In this way, the axial, $g_a(r)$, and the equatorial, $g_e(r)$, distribution functions of water molecules are defined, respectively, through

$$4\pi\rho_0(1-\cos\theta)g_a(r)r^2\Delta r = N_a(r), \tag{1}$$

$$4\pi\rho_0\cos\theta g_e(r)r^2\Delta r = N_e(r)\,, \tag{2}$$

where ρ_0 is the average density of the particles whose distribution is being computed, Δr is the binwidth of the spherical shell at a distance r of the reference point, while $N_a(r)$ and $N_e(r)$ are the number of particles in the axial and equatorial sectors of that shell. Accordingly, the usual RDF is

$$4\pi\rho_0 g(r)r^2\Delta r = N(r)\,, \tag{3}$$

where $N(r)$ is the total number of particles in the shell at r, hence, $N(r) = N_a(r) + N_e(r)$.

In order to follow the distribution of water, we will consider water oxygen (OW) whose coordinates give information on the localization of water molecules (as soon as the CM of water is close to that of oxygen). In most cases we will also analyze the distribution of water hydrogen (HW), that provide complementary information on the orientation of water molecules.

The distribution functions $g(r)$, $g_a(r)$, and $g_e(r)$ were all computed with an inhouse program developed at our lab. The total number of particles in each shell was averaged over 10^4 frames of the recorded time series. These RDFs allow to define the potential of mean force (PMF),

$$W(r) = -RT\ln g(r)\,, \tag{4}$$

where R is the universal constant of gases and T is the temperature. It allows to quantify the interactions with water. If $W(r) < 0$ (hence $g(r) > 1$), the potential is attractive (hydrophilic behavior), otherwise ($g(r) < 1$), it is repulsive (hydrophobic behavior).

C. Spatial distribution function and density maps

Complete information on the spatial patterns around reference points in the solute can be obtained through spatial distribution functions (SDFs), $g(r,\theta,\phi)$. They span both the radial and the angular spherical coordinates, rendering a full characterization of the local 3D packing of molecules.

Following the work by Kusalik and Svishchev,[13] we computed the 3D local-density histograms from the outcomes of MD simulations. We considered a frame of reference fixed at the average porphyrin ring plane with origin at the CM of the four nitrogen atoms (see Fig. 2). The space was binned in cubic cells of 1 Å linear size and its occupation at each frame of the dynamics was recorded. After suitable normalization, these histograms map the time-averaged "local density" at each cell of the 3D grid. For visualization, cuts containing the origin will be displayed.

The SDFs were also obtained by means of the program tool g_spatial in GROMACS. It was implemented as follows. The structure of the solute at the end of a MD of 500 ps with position restriction (obtained to thermalize the system previous to the useful MD) was used as the reference structure and a Cartesian system, as in Fig. 1, was attached to it. Then, at each recorded step, the whole box was centered and rotated to minimize the root-mean square deviation of the positions of the solute atoms with those of the reference structure.

Integrating over the spherical angular coordinates one can always recover the RDF. Another usual average is made by considering cylindrical coordinates and averaging over the azimuthal angle, a procedure that yields axial–radial maps. The axial–radial maps for water atoms, either oxygen (OW) or hydrogen (HW), were obtained with the g_density tool of GROMACS. The density maps were plotted by considering

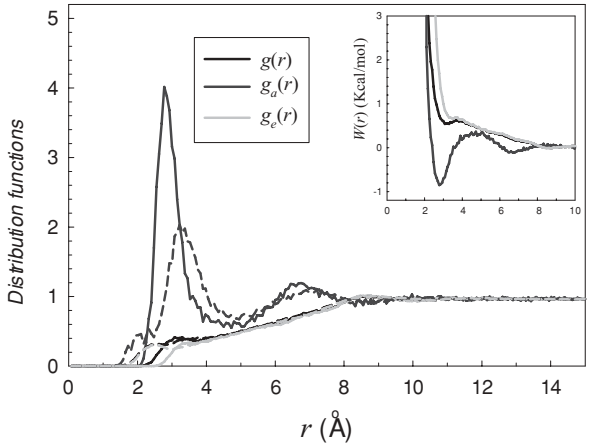

FIG. 3. Plot of $g(r)$, $g_a(r)$, and $g_e(r)$ of oxygen (OW) (full lines) and hydrogen (HW) (dashed lines) atoms of water, with respect to the CM of the nitrogen atoms in the porphyrin ring of the PPIX. $g_a(r)$ and $g_e(r)$ (for $\theta = 20^o$) exhibit the axial and equatorial contributions to $g(r)$, respectively. The inset shows the PMFs $W(r)$ given by Eq. (4), corresponding to the distribution of OW atoms.

either the x- or y-axes in Fig. 1 as the axial coordinate, while ρ is the (cylindrical) radial coordinate.

III. RESULTS AND DISCUSSION

A. Radial, axial, and equatorial distribution functions

We will analyze RDF profiles of OW atoms with reference to the CM of the four nitrogen atoms of the porphyrin ring, for PPIX and heme. The axial and equatorial contributions to the usual RDF will be uncoupled through $g_a(r)$ and $g_e(r)$, respectively. They will also be analyzed for different values of the inclination θ. The associated PMFs $W(r)$ [given by Eq. (4)] allow to quantify the energetics of the interaction of the solute with water at the different solvation shells.

In the case of PPIX (see Fig. 3), the RDF $g(r)$ becomes non-null at $r \geq 2.0$ Åand presents a first peak at $r \simeq 3.0$ Å. From visual inspection and comparison of the three profiles in Fig. 3, one concludes that the low first peak of $g(r)$ is mainly due to the contribution of the axial region, although there is also a (slightly shifted to the right) a small equatorial component. The axial profile reveals a peak at $r \simeq 6.5$ Å, which is not neat in the radial distribution nor in the equatorial profiles, where it is smeared out by the angular averaging. This is also reinforced by the increase of the peak when θ diminishes (see Fig. 4). The peak of $g(r)$ at $r \simeq 8.6$ Åis clearly associated to the equatorial region. The profiles for different values of the inclination θ collapse for $r \geq 8.6$ Å, indicating a homogeneous radial distribution of water beyond that shell.

For the heme, $g(r)$ becomes non-null at $r \simeq 2.1$ Å and has a first peak at $r \simeq 2.4$ Å (Fig. 5). Contrarily to the case of PPIX, that peak is only due to the axial portion. It is further confirmed by the change of the $g_a(r)$ profiles in Fig. 6: as the inclination θ decreases from 20° to 10°, the height of the axial peak drastically increases, differently from the case of PPIX. Moreover, the peak of $g_a(r)$ is more pronounced in the case of the heme. There is also a second peak of $g(r)$ at $r \simeq 4.4$ Å, which is absent in the case of PPIX. It originates from

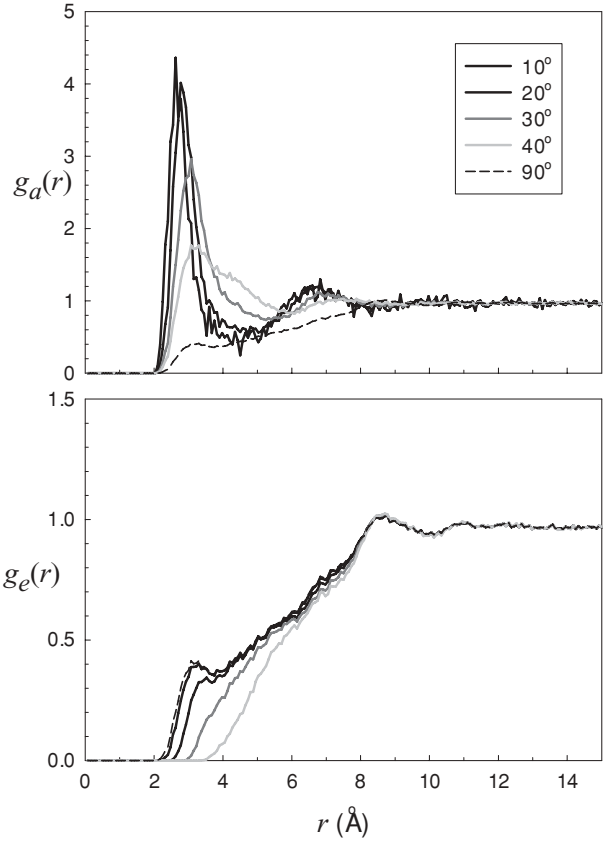

FIG. 4. Axial $g_a(r)$ and equatorial $g_e(r)$ distribution functions of OW around the center of mass of the four nitrogen atoms of PPIX, at different values of the inclination θ indicated on the figure. The usual radial distribution function was also included for comparison (dashed lines). It is recovered from $g_a(r)$ and $g_e(r)$ in the limits of $\theta = 90^o$ and $\theta = 0^o$, respectively.

the equatorial portion, since it is lacking in the axial profile (upper panel of Fig. 6) for inclinations smaller than 30°. However, the peak height in $g_e(r)$ increases when θ diminishes, suggesting a diffuse localization of water in a region with an intermediate inclination between the axis and the equatorial plane (see Fig. 6). Similarly to the case of PPIX, there is an axial peak at $r \simeq 6.5$ Å, and an equatorial one, in this case at $r \simeq 9.0$ Å. Beyond that region the profiles for different values of the cone inclination collapse as in the case of PPIX.

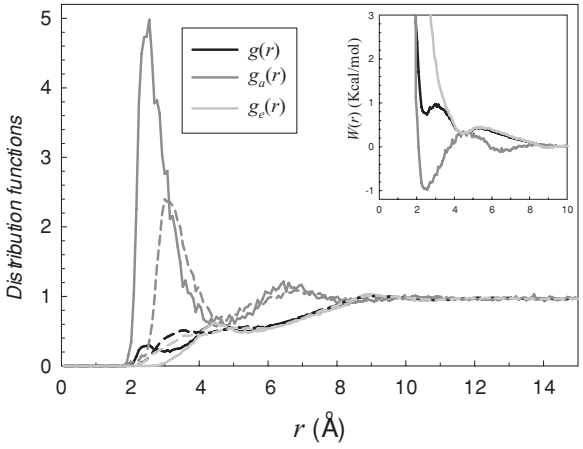

FIG. 5. Plot as in Fig. 3, for the heme.

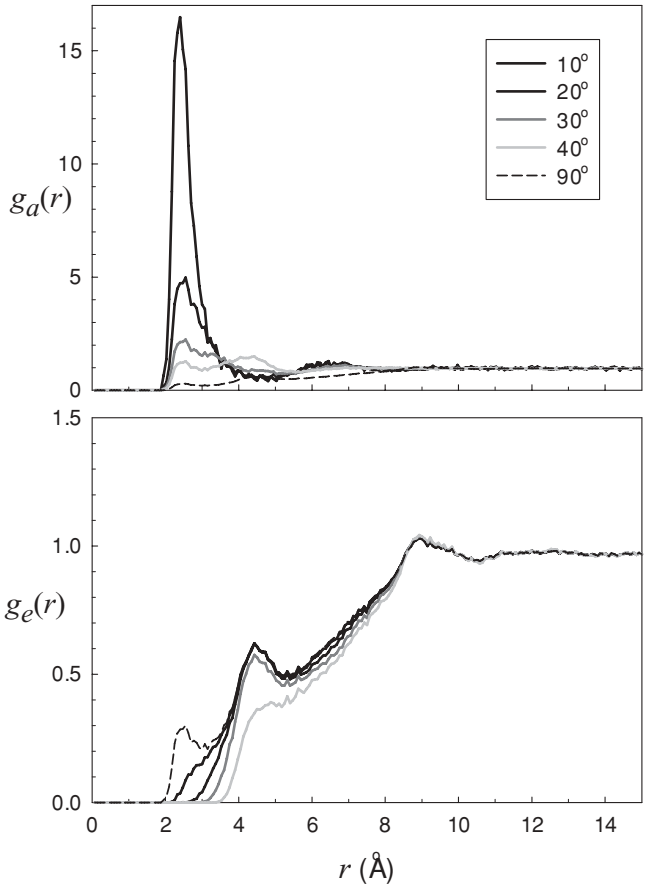

FIG. 6. Axial and equatorial distribution functions as in Fig. 4, for the heme.

The resulting profile of the $g(r)$ of heme is similar to the one previously obtained in the literature by considering as a reference point the CM of the iron atom.[4] However, it is now shifted to about +0.4 Å. This discrepancy can be assigned to the out-of-plane motion of heme iron, with an amplitude of about 0.4 Å. Recall that in the present calculation the reference point is not the CM of iron but instead the CM of the four nitrogen atoms. The localization of the peak closer to the origin in the former case suggests that water is associated to iron. In fact, *ab initio* calculations based on the density functional theory have shown that the heme iron atom maintains a charge of 0.36 and each nitrogen around it maintains an average charge of −0.055.[4] The positive charge of iron is sufficient to make (electrostatic) coordination bonds with water (one water molecule at each side of the ring).

The coordination of water with the iron atom is much more evident in the $g_a(r)$ profile, than in $g(r)$ in Fig. 5. The high first maximum of $g_a(r)$ indicates that water is well localized near iron on the axis normal to the heme ring. This effect is weaker in the case of PPIX where there is also an equatorial component. In fact, in the profiles of $g_a(r)$, in passing from 20° to 10° inclination, there is an abrupt change in the case of heme (Fig. 6), while no substantial change occurs for PPIX (Fig. 4).

Axially, the main differences between heme and PPIX are the more pronounced first peak and close proximity of the associated OW in the case of heme. The equatorial region contributes to the first peak only for PPIX and the second neat peak appears only for heme. At distances longer than about 6.5 Å, the profiles of both solutes become indistinguishable.

The complementary HW profiles in Figs. 3 and 5 display significant differences in the first peaks only, indicating that beyond the first shell water possesses unrestricted rotational mobility around their oxygen centers. Concerning the first peak, let us make the following remarks. For PPIX, the axial component diminishes and is shifted about +0.4 Å, but a lower second maximum appears at a closer radius (about 2.0 Å), while the equatorial profile is displaced about −1.0 Å. In the case of the heme, the axial component is shifted about +1.0 Å, while the equatorial peak at 4.4 Å is displaced about −1.0 Å and becomes lower and wider. In sum, HW atoms in the first equatorial shell are closer than their corresponding OW in both PPIX and heme, while HW in the first axial shell are farther than OW, but in PPIX a HW axial component closer than OW also appears. This indicates that the HW associated to the axial oxygen atoms have enhanced rotational freedom in PPIX in comparison to the heme.

From the previous analysis, one infers that the first hydration shell is formed by water molecules (at each side of the heme plane), both in the axial and equatorial regions in the case of PPIX, while closer and exclusively in the axial direction in the case of heme. Moreover, in the latter case, OW atoms are localized closer than HW ones, neatly in contrast to the case of PPIX. A second solvation shell is exclusively formed by the water localized in the equatorial region, while the third shell is axial. This last information was missing in $g(r)$ because of the angular averaging. A closer look still allows to detect an equatorial shell sector at about 9 Å.

Calculation of the PMF $W(r)$, given by Eq. (4), associated with the heme $g_a(r)$ profile (inset of Fig. 5), indicates that the free energy of a water molecule interacting with iron is about −1 kcal/mol. This potential becomes repulsive between 3.7 and 5.8 Å, while it is attractive between 5.8 and 7.2 Å, corresponding to a second axial hydration shell that is not revealed in the $g(r)$ profile with respect to the iron atom.

B. Spatial distribution function and density maps

The spatial distribution functions displayed in Fig. 7 represent the probability of finding an atom (either HW or OW) within a region of space around a molecular center. It furnishes both the radial and angular contributions. In Fig. 7, the isosurface $g(r, \theta, \phi) = 10.0$ of the SDF of water atoms surrounding the solute is displayed. In the SDF profile for the PPIX, one observes that the first hydration shell spreads along the diagonal direction defined by the nonprotonated nitrogen atoms. Moreover, water penetrates in the interstices between the carboxyls.

In the SDF for heme, the specific localization of the water is clear on the z-axis and on a torus surrounding it. While the OW atoms are localized in a reduced region of space, the corresponding hydrogen atoms occupy a more sparse region, pointing to a large orientational mobility of water molecules.

The axial–radial density maps of OW and HW around either PPIX and heme are displayed in Fig. 8. Either x or y (see Fig. 1) were alternatively taken as the axial coordinate, while ρ is the distance to the axis.

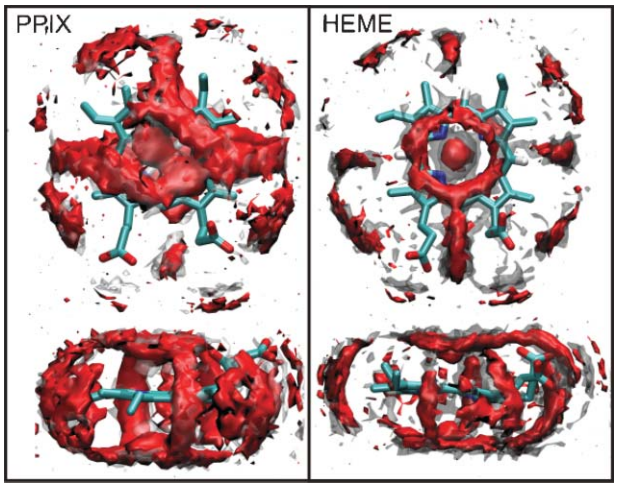

FIG. 7. Isosurfaces of the SDF of hydrogen of water (gray) and of oxygen of water (red/dark gray) with respect to PPIX and heme, for $g(r, \theta, \phi) = 10.0$. Top panels show the frontal view; bottom panels the lateral one. The plots were obtained by means of the VMD program.

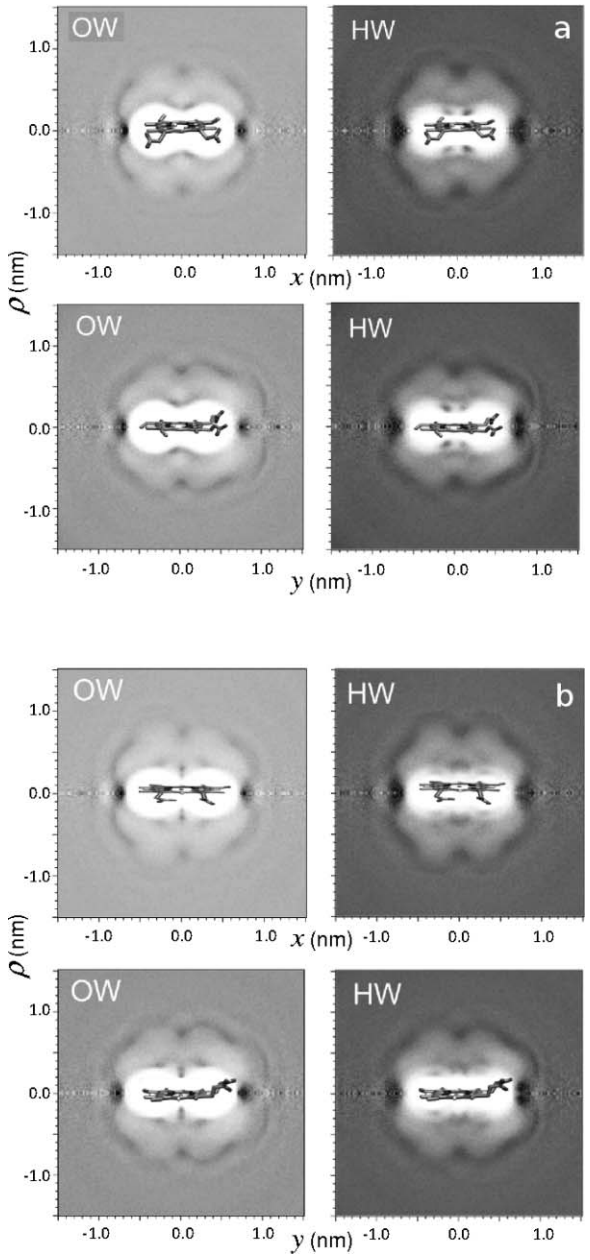

FIG. 8. Axial– radial density maps of OW and HW for PPIX [four top panels (a)] and the heme [our lower panels (b). The darker the more dense. The map for negative values of ρ is constructed by reflection. The dark regions at $\rho \simeq 0$ are spurious.

In Fig. 8(a), the HW density maps for PPIX show two dark clouds (more dense regions) at $\rho \approx 0.2$ nm in the vicinity of the central ring. They are closer to the ring than the respective clouds observed in the corresponding OW density maps, indicating that water molecules make H-bonds with the two nonprotonated hydrogen atoms of the ring. In fact, following the outcomes of *ab initio* charge calculations,[4] each nonprotonated nitrogen maintains an average charge of -0.45, that is sufficient to make H-bonds with water. The H-bonds are not necessarily formed simultaneously. The same pattern holds for both the axes, indicating four hydrogen atoms, hence four H-bonds (two at each side of the porphyrin plane), as also observed in Fig. 7, which evidences the H-bond acceptor character of the porphyrin ring (also see Table II).

In the case of heme [Fig. 8(b)], a single central cloud of higher concentration, well localized at $\rho \approx 0.3$ nm, is observed in both maps of OW. In the vicinity of the high density loci of OW, there are also high density regions of HW (now spanning a more broader region than in the case of PPIX). This portrait indicates that, differently from the case of PPIX, now (i) two water molecules are making (not necessarily simultaneously) electrostatic coordination with the iron atom, and (ii) a low mobility of the OW and higher (rotational) mobility of the corresponding hydrogen atoms.

Figure 9 exhibits the density maps on the yz and yx planes. According to Fig. 1, while yx coincides with the ring average plane, yz is normal to it and symmetric with respect to the lateral chains. For both solutes, one observes a preferential localization of water just above and below the porphyrin ring. There is also a preference for the interstitial regions, close to the C–C bonds.

Let us remark that, despite being hydrophobic solutes, both the OW and HW densities in the first shell around the porphyrins indicate enhanced probabilities of finding water molecules with respect to the bulk. MD studies of benzene[12] also show local values of water density much larger than the bulky ones, up to $5\rho_w$ (where ρ_w is equivalent to a macroscopic value of 0.0335 water molecules/Å^3). Local densities moderately larger than the bulky values have been attributed in some cases to nontetrahedral arrays of water molecules, that is, water molecules enter the tetrahedral arrays of neighboring water molecules.[13] Notice, however, that the local density we are measuring is not related to a macroscopic average number of water molecules per unit volume, but rather to a microscopic time-averaged number of particles at each cell. That is, an actual local density calculation should rely on counting particles on a volume small compared to the whole system but large enough to contain a large number of particles. However, in order to obtain local information on the localization of water molecules we have chosen 1 Å^3 grid

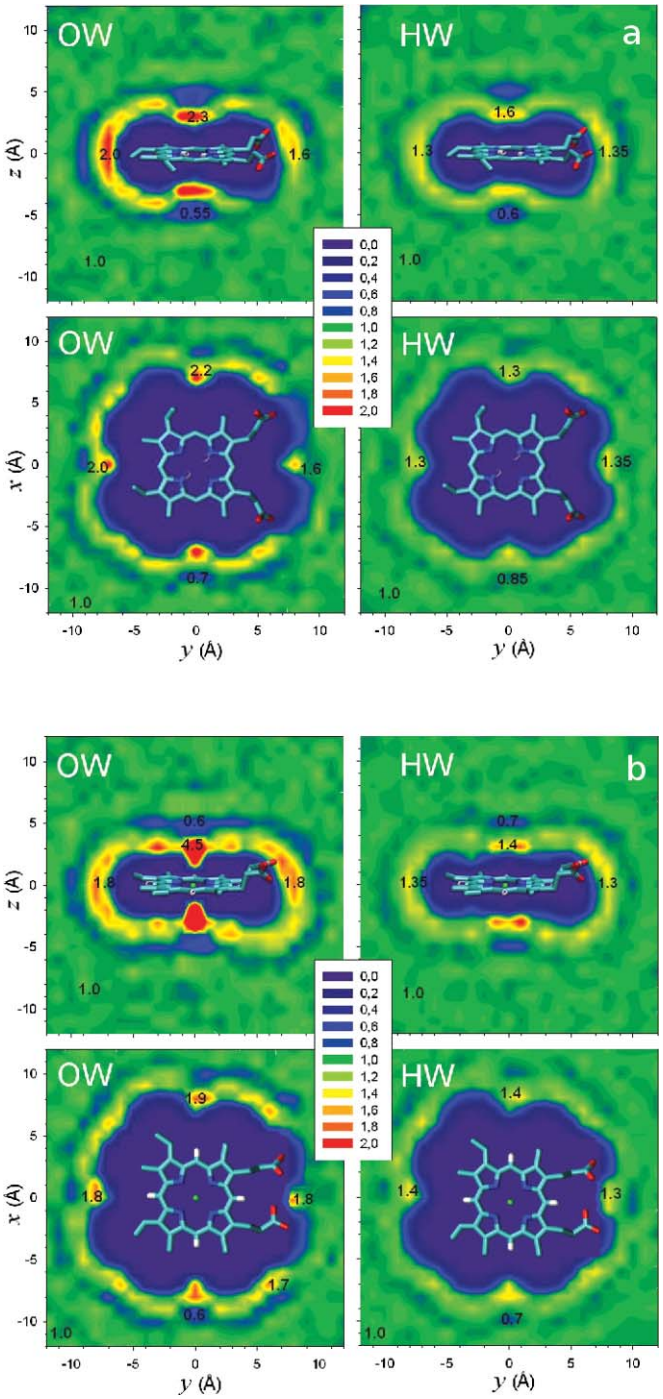

FIG. 9. OW and HW densities around PPIX (a) and heme (b). Histograms, with cubic bins of 1 Å linear size, were built with the positions of either OW or HW atom centers. Cuts containing the origin of coordinates are displayed. Density is normalized by the bulky value equivalent to a macroscopic density of 0.0335 water molecules/Å^3.

cells, that hence, will be either empty or occupied by at most one OW at each frame of the dynamics. Therefore, the obtained "density" should be interpreted as proportional to the probability of the occupation of each small cell of the grid, relative to the bulk. Then, for instance, $4\rho_w$ would mean that the dwelling time in the cell is four times larger than in the bulk (implying larger immobilization in that cell) and not necessarily that water molecules are more tightly packed.

In the first solvation shell of PPIX, the density of OW attains, in the region close to the C–C bonds of the porphyrin ring values, around twice that of the bulk density ρ_w. Meanwhile, in those regions, the density of HW is lower although still larger than ρ_w. This indicates that OW has more restricted positions than HW, which possesses rotational freedom. In the vicinity of the lateral chains, one observes a OW density around $1.3\rho_w$. In the valley between the first and second hydration shells, the density is slightly lower than the bulk density, around $0.8\rho_w$, while the second shell has a mean density of about $1.2\rho_w$.

In the case of heme, the density close to the C–C bonds of the hydrophobic core is slightly larger than for PPIX (about $1.7\rho_w$). But the main difference is found in the closer proximity and immobilized of OWs near the centroid of the porphyrin ring, which is associated to the coordination with the heme iron atom.

C. Fluctuations in hydration shells

To gain insights on the occupation of water in the solvation shell of the whole solute, the number of water molecules at distance shorter than a given value d from the solute was computed as a function of time. Its time average and standard deviation were calculated for each solute. Then, local normalized fluctuations

$$F = \frac{\langle N^2 \rangle - \langle N \rangle^2}{\langle N \rangle}, \tag{5}$$

were also computed. The extent of fluctuations can be used as a measure of hydrophobicity.[14] Moreover, the fluctuation of the number of water molecules is related to the isothermal compressibility, and hence, rules the sensitivity to pressure.

Figure 10 shows the fluctuations in the average number of water molecules (OW), at a distance smaller than d from each solute. Additionally, the average differential number $\langle n \rangle$, such that $\langle N \rangle(d) = \int_0^d \langle n(x) \rangle dx$ is also displayed. Both solutes present similar average cumulative number of OW atoms as a function of the distance to the solute as well as very similar fluctuations. Near the solutes, the values of F are larger than the bulky one. The obtained bulk value is compatible with those previously obtained under similar pressure and temperature conditions.[14] An enhanced amplitude of the fluctuations in the vicinity of a hydrophobic solute is expected. Notice, however, the nonmonotonic decay of F with the distance to the solute surface, presenting a local maxima at the hydration shells, before attaining the bulky value. The extent of fluctuations has been proposed as a measure of the degree of hyphobicity.[14] On the other hand, it also depends on the size of the hydrophobic solute. Then, since the surface areas (see Table I) of both solutes are comparable, they present a similar degree of hydrophobicity, as measured by F, at the different shells.

D. H-bonds

H-bonds between porphyrin and water molecules were computed using the code g_hbond of GROMACS4.0, with a correction to avoid double counting. In this program,

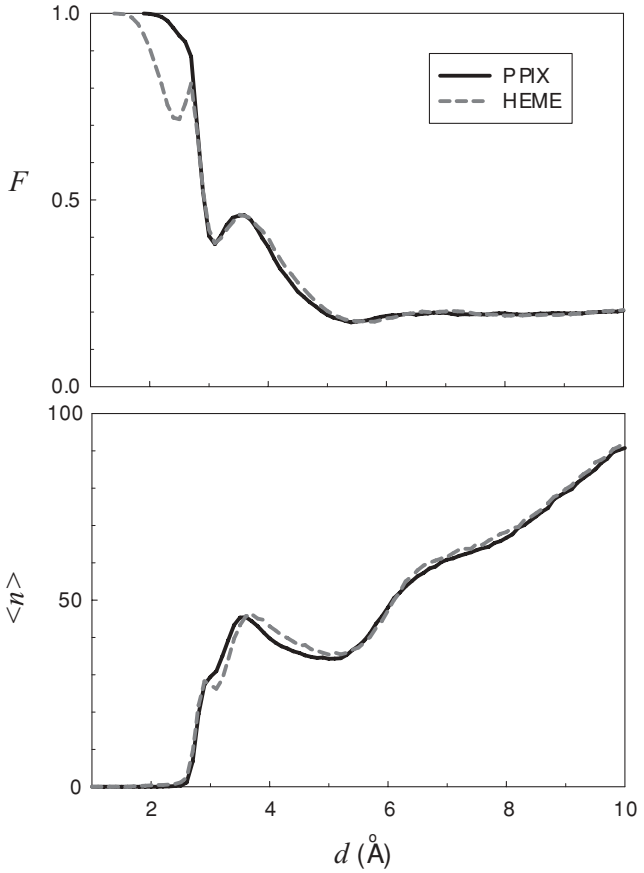

FIG. 10. Normalized fluctuations of the number of OW at a distance smaller than d from the solute (upper panel) and differential number of OW as a function of d (lower panel).

calculations are based on the "intermittent H-bond correlation function," that was developed to be insensitive to the rate of data recording. By means of this scheme we found the time-averaged number of H-bonds that each porphyrin (and each atom of the molecule) forms with water, showing the proportion of donor and acceptor atoms in porphyrins.

The outcomes confirm the results found both in the density maps and in the plots of SDFs where one observes that, despite the hydrophobic character of PPIX resides in the central ring, it has the capacity of establishing H-bonds with water, acting as a whole as a H acceptor.

Table II shows that PPIX forms in average about 10% more H-bonds than heme and that the nonprotonated nitrogen in PPIX are the main responsible for that difference.

TABLE I. Time-averaged surface area in nm^2. Hydrophobic and hydrophilic surfaces are distinguished, obtained with g_sas of GROMACS Ref. 15.

	PPIX	Heme
Hydrophobic	5.56 ± 0.19	6.04 ± 0.18
Hydrophilic	1.84 ± 0.13	1.57 ± 0.12
Total	7.41 ± 0.23	7.62 ± 0.22

TABLE II. Time-averaged number of H-bonds (per atom) formed with each class of atoms for PPIX and heme. The total number of H-bonds is also shown for each solute (last row).

Atom	PPIX	Heme
N	0.7 ± 0.4	0.2 ± 0.2
NH	0.1 ± 0.2	...-
O	2.2 ± 0.3	2.2 ± 0.3
All	10.3 ± 1.4	9.3 ± 1.3

IV. COMPARISON WITH OTHER MODELS

In order to check the robustness of the result with respect to changes in the chosen models, we performed simulations for the heme also in the all-atom force-field CHARMM27. We also considered different water models (SPC, SPCE, TIP3P, and TIP4P) available in the GROMACS package for the CHARMM27 force-field. The results of the comparison are illustrated in Figs. 11 and 12, for the distribution of OW and HW, respectively.

While no significant differences are observed for different water models, the CHARMM27 and GROMACS96 models

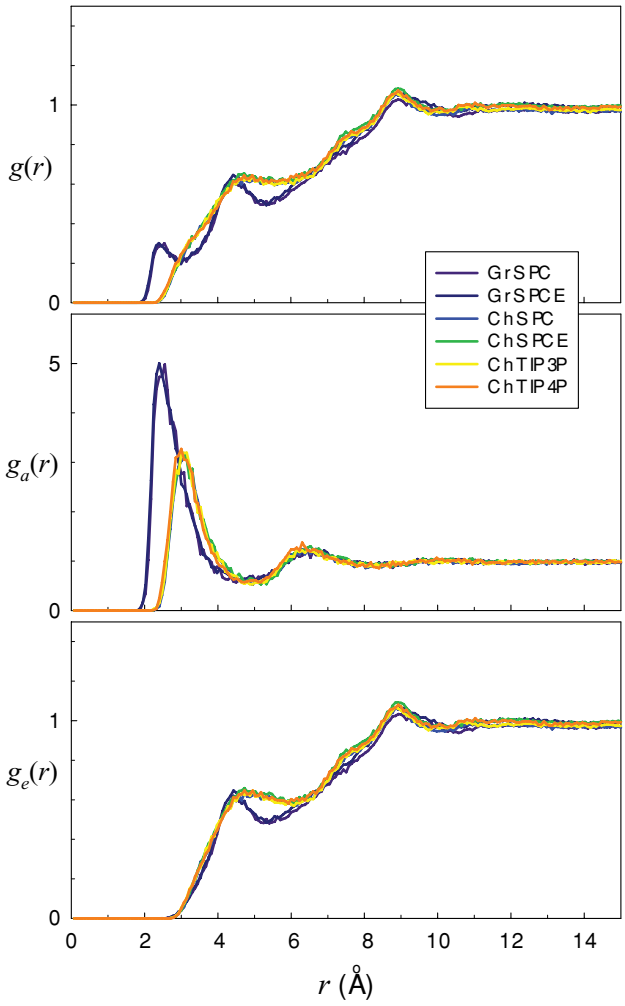

FIG. 11. Plot of $g(r)$, $g_a(r)$, and $g_e(r)$ of oxygen (OW) for the different models of heme [GROMOS96 (Gr) and CHARMM27 (Ch)] and water (SPC, SPCE, TIP3P, and TIP4P) indicated on the figure. $g_a(r)$ and $g_e(r)$ were computed for $\theta = 20^o$.

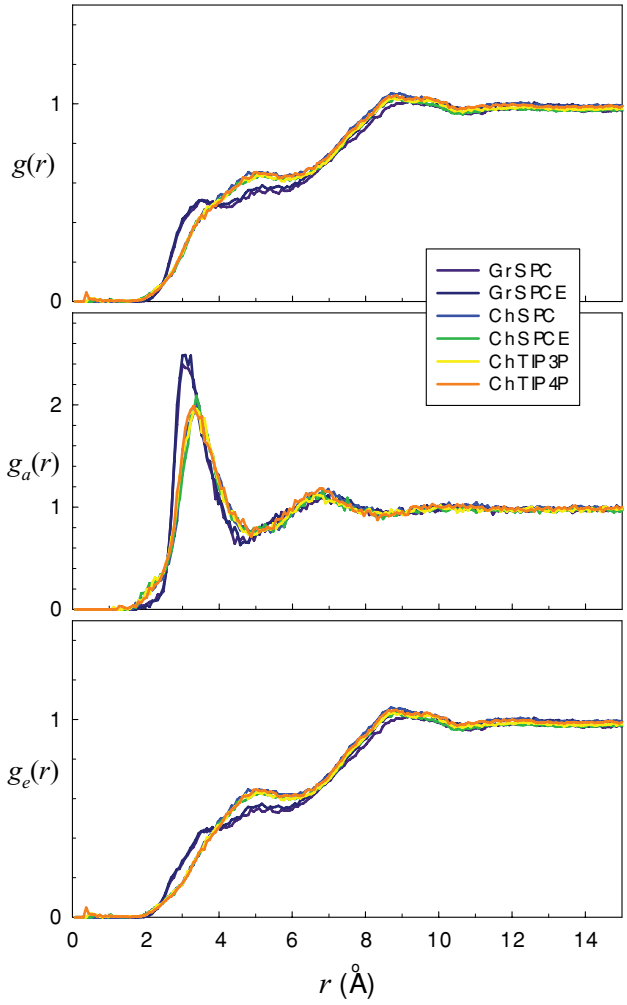

FIG. 12. Plot of $g(r)$, $g_a(r)$, and $g_e(r)$ of hydrogen (HW) for the different models of heme [GROMOS96 (Gr) and CHARMM27 (Ch)] and water (SPC, SPCE, TIP3P, and TIP4P) indicated on the figure. $g_a(r)$ and $g_e(r)$ were computed for $\theta = 20^o$.

for the solute display differences as expected. Discrepancies in the structure of the radial profile can be understood from the decomposition in axial and equatorial components. In the all-atom model, the first peak in the axial distribution of OW is shifted in about +1 Å and its intensity decreases indicating larger mobility of the axially localized oxygen atoms OW, while the profile beyond 5Å is unaffected. Also, the second peak of the radial profile, related to the equatorial contribution, is smoothed. Meanwhile, the HW profiles display less pronounced differences.

V. CONCLUSIONS AND FINAL REMARKS

The interactions between biomolecules are often mediated by solvents. The structure and fluctuations of the solvation layers around porphyrins are, therefore, crucial to determine their binding and reactivity. We have examined the nonuniform hydration in the vicinity of PPIX and heme, two biologically relevant hydrophobic molecules.

In principle, a detailed description of the vicinity of Fe would require a quantum mechanical treatment.[16] It has been reported that transition metal ions (in particular, Fe^{3+}) induce water dissociation, which change the solvent structuring around them.[17] However, the central part of the heme does not present a net charge. Charge transfer is also important.[18] Then, the present approach is limited in that respect. But, although we had chosen a reference frame located at the centroid of the ring, because of its geometric privileged position, we aim to study the organization of water around the solute as a whole, and not particularly the problem of water coordination with Fe. Then, we think that the classical approach can be quite accurate for our purpose. In any case, our results constitute a reference for comparison with future work using more sophisticated models.

The complementary information provided by partially integrated distribution functions and density maps around the centroid of the porphyrin ring was explored. The first hydration layer typically corresponds to water molecules making H-bonds with the solute. Although PPIX is a hydrophobic molecule, the axial–radial density maps reveal H-bonds between the water and the nonprotonated nitrogen atoms in the hydrophobic core. As shown in Table II, there is a tendency that the porphyrin center acts as a weak acceptor of water hydrogen atoms. Despite its localization in the porphyrin ring, the central nitrogen atoms form intermittent H-bonds with water.

In PPIX, there is a preferential occupation of water close to the nonprotonated nitrogen atoms of the porphyrin ring. In the case of heme, the first layer has a preferential axial occupation. The axial distribution function spanning an angle $\theta = 20^o$ reveals a well oriented electrostatic coordination of iron with water oxygen. A solvation layer at around 6.5 Å, that was not evident in the $g(r)$ plot, was revealed by the $g_a(r)$ profile. The axial oxygen atoms present a low mobility in comparison with their associated hydrogen atoms. Analysis of the PMF shows that the free energy of the water molecule interacting axially with iron is approx. −1 kcal/mol. Moreover, the SDF shows that the interstitial C–C bond regions that form the porphyrin ring are penetrated by water. This has also been observed in other hydrophobic molecules.[12]

We found time-averaged local densities ranging between 0.6–4.0ρ_w. Water densities in some regions surrounding the solutes (see Fig. 9) are up to several times larger than the bulky values. As discussed in Sec. III B, time-averaged local densities taking values several times the bulky ones rather reflect the local immobilization of water molecules rather than tighter packing. The present work shows a further example of the unusual high probability of finding water molecules in the vicinity of hydrophobic solutes.

The dependence of the results on the chosen modeling was checked through alternative force fields for water and the heme. We performed simulations with SPC/E (available in the GROMACS96 GROMACS package) and observed no significant differences between both water models. We also considered an all-atom model for the solute (standard parameterization of CHARMM27 in the GROMACS package) and the water models available at the GROMACS package (SPC, SPCE, TIP3P, and TIP4P). No significant differences were found amongst these cases neither. Of course, close to the solute, differences are found between the united-atom and

all-atom models. However, they are clearly delimited and consistent with the addition of methyl hydrogen atoms. Moreover, the differences are found mainly in the distribution of OW, while not significantly in the distribution of HW.

It is interesting that the simple model GROMACS96+ SPC already displays the same features of water organization around the solute as force fields with higher level of detail. This is an important finding to be considered in designing simulations involving larger systems, specially because the chosen model represents a widely used combination adopted in MD simulations of biomolecules. This may be of help for interpreting both past and future work modeling these systems as well as its comparison with experimental results. Moreover, the present picture of the organization of water around the heme, which is so important for the function and activity of heme proteins, represents a basis for comparison with future work using more sophisticated modeling.

ACKNOWLEDGMENTS

We acknowledge Brazilian agencies Faperj (Foundation for Research Support, State of Rio de Janeiro) and CNPq (National Council for Scientific and Technological Development) for financial support. We also acknowledge the developers of free softwares without which the present work would not have been possible.

[1]A. K. Singh, N. Singh, M. Sinha, A. Bhushan, P. Kaur, A. Srinivasan, S. Sharma, and T. P. Singh, J. Biol. Chem. **284**, 20311 (2009).
[2]D. C. Haines, D. R. Tomchick, M. Machius, and J. A. Peterson, Biochemistry **40**, 13456 (2001).
[3]P. A. Zunszain, J. Ghuman, T. Komatsu, E. Tsuchida, and S. Curry, BMC Struct. Biol. **3:6** (2003), see http://www.biomedcentral.com/1472-6807/3/6.
[4]T. R. Cuya Guizado, S. da Rocha Pita, S. R. W. Louro, and P. G. Pascutti, Int. J. Quantum Chem. **108**, 2603 (2008).
[5]T. R. Cuya, S. R.W. Louro, P. G. Pascutti, and C. Anteneodo, Int. J. Quantum Chem. **110**, 2094 (2010).
[6]D. van der Spoel, E. Lindahl, B. Hess, C. Kutzner, A. R. van Buuren, E. Apol, P. J. Meulenhoff, D. P. Tieleman, A. L. T. M. Sijbers, K. A. Feenstra, R. van Drunen, and H. J. C. Berendsen, GROMACS *User Manual Nijenborgh* (Groningen University, The Netherlands, 2002).
[7]H. J. C. Berendsen, J. P. M. Postma, W. F. van Gunsteren, and J. Hermans, *Intermolecular Forces*, edited by B. Pullman (D. Reidel, Dordrecht, The Netherlands, 1981).
[8]H. J. C. Berendsen, J. R. Grigera, and T. P. Straatsma, J. Phys. Chem. **91**, 6269 (1987).
[9] W. L. Jorgensen, J. Chandrasekhar, J. D. Madura, R.W. Impey, and M. L. Klein, J. Chem. Phys. **79**, 926 (1983).
[10]U. Essmann, L. Perera, M. L. Berkowitz, T. Darden, H. Lee, and L. G. Pedersen, J. Chem. Phys. **103**, 8577 (1995).
[11]H. J. C. Berendsen, J. P. M. Postma, A. DiNola, and J. R. Haak, J. Chem. Phys. **81**, 3684 (1984).
[12]T. M. Raschke and M. Levitt, J. Phys. Chem. B **108**, 13492 (2004).
[13]P. G. Kusalik and I. M. Svishchev, Science **265**, 1219 (1994).
[14]S. Sarupria and S. Garde, Phys. Rev. Lett. **103**, 037803 (2009).
[15]This tool uses the Connolly algorithm with a 0.14 nm radius for the solvent probe: M. L. Connolly, Science **221**, 709 (1983).
[16]O. Coskuner, D. E. Bergeron, L. Rincon, J. W. Hudgens, and C. A. Gonzalez, J. Phys. Chem A **113**, 2491 (2009).
[17]O. Coskuner, E. A. A. Jarvis, and T. C. Allison, Angew. Chem. Int. Ed. **46**, 7853 (2007).
[18]K. Leung, I. M. B. Nielsen, N. Sai, C. Medforth, and J. A. Shelnutt, J. Phys. Chem A **114**, 10174 (2010); K. Leung and C. J. Medforth, J. Chem. Phys. **126**, 024501 (2007).